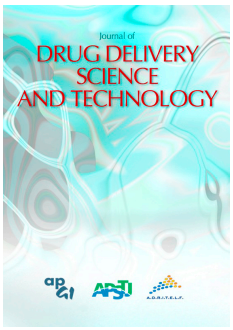

4D Printing of Shape-Memory Polymer-Based Floating Tablets via Fused Deposition Modelling: Transformable Helical Structure to Tablet-Like Form

Pattaraporn Panraksa, Sherif I. Hamdallah, Ozkan Yilmaz, Phennapha Saokham, Pornchai Rachtanapun, Sheng Qi, Pensak Jantrawut

PII: S1773-2247(24)01203-6

DOI: https://doi.org/10.1016/j.jddst.2024.106534

Reference: JDDST 106534

To appear in: *Journal of Drug Delivery Science and Technology*

Received Date: 8 September 2024

Revised Date: 28 November 2024

Accepted Date: 12 December 2024

Please cite this article as: P. Panraksa, S.I. Hamdallah, O. Yilmaz, P. Saokham, P. Rachtanapun, S. Qi, P. Jantrawut, 4D Printing of Shape-Memory Polymer-Based Floating Tablets via Fused Deposition Modelling: Transformable Helical Structure to Tablet-Like Form, *Journal of Drug Delivery Science and Technology*, https://doi.org/10.1016/j.jddst.2024.106534.

Predesigning
in CAD software

Eight helical models
with different

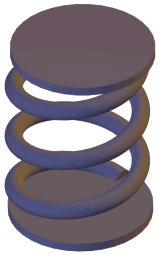

Helix diameter
(1.0 mm, 1.5 mm)

Number of helical turns
(2 turns, 3 turns)

Top/base height
(0.5 mm, 1.0 mm)

Fused deposition modeling
(FDM) 3D Printing

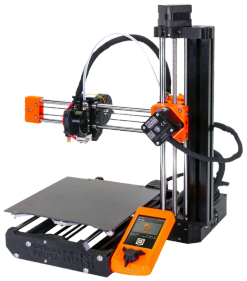

- Geometric accuracy
- Thermal analysis and Programming of temporary tablet-like shape at Tg + 5 °C (65 °C) (Heating, deformation, and cooling)
- Shape-memory performance

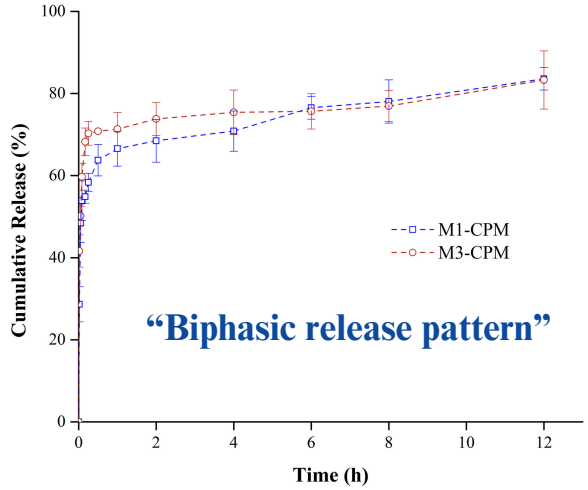

"Tablet-like shape"

"Recovery helical model"

M1

M3

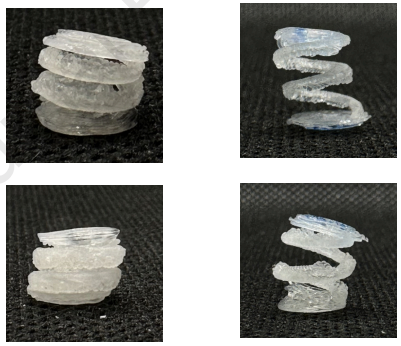

The optimal models was selected.

- Drug loading via soaking method
- Characterisation of the drug-loaded models
- Floating behaviour
- *In vitro* release study

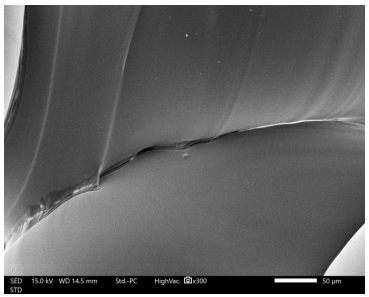

Non-drug-loaded
surface morphology

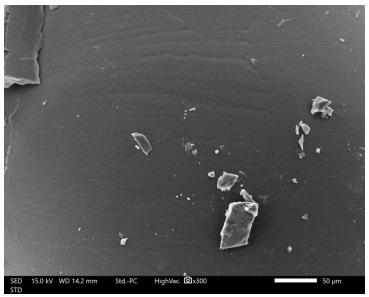

Drug-loaded
surface morphology

"Shape recovery of drug-loaded models"

M1-CPM M3-CPM

4D Printing of Shape-Memory Polymer-Based Floating Tablets via Fused Deposition Modelling: Transformable Helical Structure to Tablet-Like Form

Pattaraporn Panraksa [a], Sherif I. Hamdallah [b,c], Ozkan Yilmaz [b], Phennapha Saokham [a], Pornchai Rachtanapun [d,e,f], Sheng Qi [b], and Pensak Jantrawut [a,e,f,*]

[a] *Department of Pharmaceutical Sciences, Faculty of Pharmacy, Chiang Mai University, Chiang Mai 50200, Thailand; pattaraporn.prs@gmail.com, pattaraporn.pan@cmu.ac.th (P.P.); phennapha.s@cmu.ac.th (P.S.)*

[b] *School of Pharmacy, University of East Anglia, Norwich NR4 7TJ, UK; ozkanyilmaz235@gmail.com (O.Y.); s.hamdallah@uea.ac.uk (S.H.); sheng.qi@uea.ac.uk (S.Q.)*

[c] *Department of Pharmaceutics, Faculty of Pharmacy, Alexandria University, Alexandria, Egypt*

[d] *Division of Packaging Technology, School of Agro-Industry, Faculty of Agro-Industry, Chiang Mai University, Chiang Mai 50100, Thailand; pornchai.r@cmu.ac.th (P.R.)*

[e] *Center of Excellence in Materials Science and Technology, Chiang Mai University, Chiang Mai 50200, Thailand*

[f] *Center of Excellence in Agro Bio-Circular-Green Industry (Agro BCG), Agro-Industry, Chiang Mai University, 155 Mu 2, Mae-hea, Muang, Chiang Mai 50100, Thailand*

*Corresponding author.

E-mail address: pensak.amuamu@gmail.com, pensak.j@cmu.ac.th (P.J.).

ABSTRACT

The integration of four-dimensional (4D) printing technology into pharmaceutical manufacturing has introduced a transformative approach to drug delivery systems, offering flexible alternatives to improve drug bioavailability. This study advanced the field by developing an innovative 4D-printed floating drug delivery system using Fused Deposition Modelling (FDM) and a temperature-responsive polymer, polylactic acid (PLA). Unlike traditional methods and previous literature that relied on external devices or encapsulation, our approach utilised the shape-memory properties of PLA to create helical structures that transform into tablet-like forms when heated and subjected to an external force. Under gastric conditions, these structures reverted to their original shape, allowing them to float and release drugs over an extended period. In this work, eight helical models (M1 to M8), were designed and fabricated with varying geometric parameters, including helix diameter, number of helical turns, and top/base height, to assess their geometric accuracy, shape-memory performance, drug-loading efficiency, floatability, and release behaviour. Results showed that models with smaller helix diameters and fewer turns exhibited superior shape recovery, with the highest observed at 79.5% for Model M1 (1.0 mm helix diameter, two helical turns, and 0.5 mm top/base height). Meanwhile, models with larger diameters showed higher drug-loading capacities. Additionally, the drug-loaded models demonstrated significant shape-recovery and floating performances, suggesting the potential for prolonging drug release for up to 12 h. These findings highlight the potential of 4D printing in developing advanced drug delivery systems, providing new insights into how this technology can improve drug administration and drug delivery through shape-changing tailored systems.

Keywords: Additive manufacturing; 4D printing; 3D printing; Fused deposition modelling; Gastroretentive drug delivery system; Floating drug delivery system; Shape-memory polymer

Highlights

- A novel 4D-printed floating drug delivery system was developed.
- Drug Delivery System utilises PLA-based helical structures for shape transformation.
- Helical constructs transform in response to temperature changes.
- Geometric parameters crucially influence shape-changing performance.

1. Introduction

Solid oral dosage forms, including powders, granules, capsules, and tablets, are among the most widely used platforms of drug delivery due to their stability, ease of production, cost-effectiveness, and high patient adherence [1,2]. Their convenience makes them a preferred choice for self-administered medications in clinical settings. However, the complex and variable environment of the gastrointestinal (GI) tract poses significant challenges for effective drug delivery [3,4]. Fluctuating pH levels in different GI segments, variable mucus layer thickness, residence time, and the presence of gut bacteria all profoundly impact drug absorbability and bioavailability [5–7]. For example, the stomach's acidic environment (pH 1-2.5) can degrade many drug molecules, thereby reducing their efficacy. Additionally, first-pass metabolism, where the drug is metabolised in the liver after absorption, leads to a significant loss of the administered dosage. Other challenges include short gastric residence time, inconsistent gastric emptying, and the need for frequent dosing of drugs with short half-lives [8]. These factors, combined with mechanical stresses from peristalsis and osmotic pressure, further reduce drug absorption and therapeutic effectiveness [4]. To address these challenges and improve drug bioavailability, innovative drug delivery systems, such as gastro-retentive drug delivery systems (GRDDS), have been developed. GRDDS are designed to extend the gastric residence time and enable prolonged drug release, especially for drugs with a narrow absorption window in the stomach. These systems help overcome absorption-related challenges within the GI tract, ultimately leading to better therapeutic outcomes. A diverse array of GRDDS have been developed, encompassing high-density [9], expandable [10], magnetic [11], mucoadhesive [12], and floating systems [13,14]. Among these, floating systems have garnered significant attention within pharmaceutical research and industry. By being less dense than gastric fluids, they remain buoyant in the stomach for extended periods, significantly enhancing the bioavailability of drugs absorbed in the stomach or upper small

intestine. Traditionally, floating systems have been fabricated from materials such as polypropylene foams and oils, but these offer limited material versatility [15,16].

Three-dimensional (3D) printing is one type of additive manufacturing (AM) that has evolved significantly over the past few decades, with applications spanning industries like automotive, aerospace, biomedical, and pharmaceuticals [17]. Among the various techniques, binder jet 3D printing (BJ-3DP), fused deposition modelling (FDM), semi-solid extrusion (SSE), and stereolithography (SLA) stand out for their potential to develop personalised drug delivery systems [18]. These technologies allow for the creation of complex dosage forms that were once impossible to achieve through traditional methods or would have required costly multi-stage processes. Moreover, 3D printing enables personalised medicine by allowing pharmacists to create formulations tailored to individual patient needs, incorporating precise amounts of active pharmaceutical ingredients (APIs) [19].

Building on the success of 3D printing, the novel concept of four-dimensional (4D) printing introduces time as a critical factor. This approach utilises smart materials–such as shape-memory alloys (SMAs), shape-memory polymers (SMPs), and stimuli-responsive gels–that can change their structure or functionality when exposed to external stimuli like light, temperature, solvents, magnetic fields, enzymes, or pH [20,21]. This dynamic behaviour has significant implications for drug delivery systems, enabling them to adapt to physiological conditions and enhance therapeutic outcomes. Shape-memory polymers (SMPs) are particularly promising for 4D printing applications in biomedical and pharmaceutical fields, as they can be programmed to transition between temporary and permanent shapes in response to specific stimuli [22–25]. For example, temperatures-responsive SMPs, such as polyvinyl alcohol (PVA), polyurethane (PU), crosslinked methacrylate poly(caprolactone), and polylactic acid (PLA), can be deformed into a temporary shape above their glass transition temperature (T_g) and then recover their original shape when triggered by heat [26]. Despite the

growing promise of 4D printing, its application in pharmaceutical formulation development is still in its early stages, with limited studies reported. For instance, Uboldi et al. [27] developed expandable bladder-retentive drug delivery systems using PVA-based SMPs, which recovered 70% of their original shape when exposed to simulated urine at 37 °C for 3 min. Similarly, Melocchi et al. [28] fabricated a PVA-based expandable GRDDS through FDM, programmed into a supercoiled temporary shape for insertion into capsules. Upon immersion in hydrochloric acid (HCl), the capsule disintegrated, allowing the system to expand and recover its original shape. These examples highlight the ability of 4D-printed systems to transform within the body, but they often rely on external devices, such as capsules, for drug delivery.

In this study, we aim to advance the concept of shape-transforming drug delivery by developing a novel 4D-printed floating system that can be administered directly without the need for additional devices, using an FDM printer with a temperature-responsive polymer. Unlike previous approaches that require additional devices such as capsules, our method utilises polylactic acid (PLA) to create helical structures that can transform into a tablet-like form when subjected to heat and external force. Once exposed to gastric conditions, this tablet can revert to its helical shape, enabling it to float in the stomach for prolonged period. This novel approach not only simplifies the drug delivery process by eliminating the need for capsules or additional devices but also has the potential to enhance gastric retention and prolong drug release, particularly for acid-stable drugs, ultimately overcoming common challenges in oral drug delivery.

2. Material and Methods

2.1. Materials

Polylactic acid (PLA) filament with a diameter of 1.75 ± 0.05 mm and a density of 1.24 g/cm^3 was purchased from eSun®, Shenzhen Esun Industrial Co., Ltd. (Shenzhen, China). Chlorpheniramine maleate ($C_{20}H_{23}ClN_2O_4$, molecular weight 390.9 g/mol), the model drug used in this study, was purchased from S. Tong Chemicals Co., Ltd. (Nonthaburi, Thailand). Ethanol (95.0%) was purchased from Liquor Distillery Organization Thailand (Chachoengsao, Thailand). 1 N Hydrochloric acid solution (AR grade) was purchased from RCI Labscan Ltd. (Bangkok, Thailand). All other chemicals and reagents used in this study were of analytical grade to ensure consistency and reliability in experimental results.

2.2. CAD Design and Fused Deposition 3D printing of the Helical Models

To design floating drug delivery systems that are both effective and patient-friendly, we focused on creating helical structures for several key reasons. Helical geometries are easily compressed, which allows them to be formed into tablet-like shapes that are easier for patients to swallow. Once ingested, these structures expand back into their helical shape and can float in gastric fluids, extending their residence time in the stomach and enhancing drug absorption. The balanced helical form further provides the necessary buoyancy for prolonged gastric retention while allowing for sustained drug release. In this study eight helical constructs were designed using AutoCAD® 2024 software (Autodesk Inc., San Francisco, CA, USA). The geometric parameters varied across models, including helix diameter, number of helical turns, and top/base height, as detailed in Table 1 and illustrated in Fig. 1, in order to explore the influence of geometric parameters on the shape-memory properties, floating ability, and release behaviour of models. Each construct was standardised with a base diameter of 8.0 mm and a helical part height of 10.0 mm to ensure consistent comparison across models.

147 **Table 1.** Geometric parameters for the fabrication of the eight helical constructs.

Model code	Helix diameter (mm)	No. of helical turns	Top/Base height (mm)
M1	1.0	2	0.5
M2	1.0	3	0.5
M3	1.5	2	0.5
M4	1.5	3	0.5
M5	1.0	2	1.0
M6	1.0	3	1.0
M7	1.5	2	1.0
M8	1.5	3	1.0

148 After finalising the CAD geometries, the models were exported as stereolithography
149 (.stl) files. These .stl files were subsequently sliced into layers using PrusaSlicer software
150 version 2.7.4 (Prusa Research, Prague, Czech Republic), which is based on the open-source
151 Slic3r software developed by Alessandro Ranellucci and the RepRap community. This slicing
152 process generated the necessary G-code for 3D printing. The following printing parameters
153 were carefully set to optimise print quality and ensure the structural integrity of the helical
154 constructs. The nozzle temperature was set at 205 °C for the first layer and 200 °C for
155 subsequent layers. The bed temperature was maintained at 60 °C. The first layer height was set
156 at 0.2 mm, while the remaining layers were printed at a height of 0.07 mm. The models were
157 printed with three perimeters, a 0% infill density, and a 45° fill angle. The printing speed was
158 maintained at 40 mm/s, with a nozzle travelling speed of 150 mm/s. The brim setting and
159 support function mode ‘For support enforcers only’ were enabled to maintain the adherence of
160 the 3D models to the build plate and the stability of complex structures during printing. The
161 3D models were then fabricated using a fused filament fabrication (FFF) technique on an
162 Original Prusa Mini+ FDM 3D printer (Prusa Research, Prague, Czech Republic) equipped
163 with a 0.4 mm nozzle.

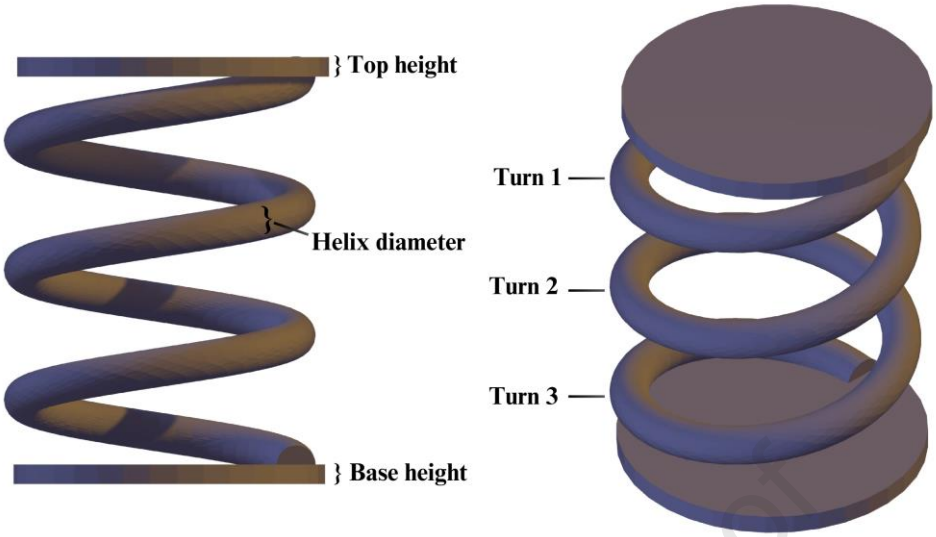

164

165 **Fig. 1.** Graphical illustration showing the definition of helix diameter, number of helical turns, and base height.

166

167 *2.3. Evaluation of Printing Fidelity and Weight Variation of 3D-Printed Helical Models*

168 In this study, we focused on assessing the helix diameter as the primary geometric
169 parameter to ensure the printing quality and reproducibility of the 3D printing process. The
170 helix diameter is particularly crucial as it can significantly affect dimensional stability,
171 mechanical performance and functional integrity of the final product, as highlighted in prior
172 studies [29]. For this study, images of both side views of the 3D-printed helical constructs,
173 fabricated via FDM, were captured using a digital portable USB microscope (Yao, Shenzhen,
174 China) equipped with 8 LED lights and a high-definition Complementary Metal Oxide
175 Semiconductor (CMOS) sensor. The images were acquired using camera software for
176 Windows 10 with a resolution of 640 pixels (Microsoft Corporation, Redmond, WA, USA).
177 The microscope was positioned at a fixed distance of 5.0 cm from the samples to ensure
178 consistency across measurements. The helix diameter of each model was measured in triplicate
179 on both sides using the image processing tool (ImageJ software version 1.54g, National
180 Institutes of Health (NIH), Bethesda, MA, USA). Printing fidelity was then quantified through

the comparison of actual printed dimensions against the designed dimensions from the CAD model.

Additionally, the weight variations of all models were assessed to further confirm the reproducibility of the 3D printing. Ten of each model were randomly chosen and individually weighed using an analytical balance with a readability of 0.0001 g (LAB 214i, Adam Equipment Co. Ltd., Kingston, Milton Keynes, UK).

2.4. Shape-Memory Effect of 3D-Printed Helical Models

2.4.1. Thermal Analysis via Differential Scanning Calorimetry

The thermal properties of the PLA filament were characterised using a differential scanning calorimetry (DSC) instrument (DSC 1 Module, Mettler-Toledo Sales International GmbH, Greifensee, Switzerland), with data analysed via STAR^e software version 16.40. For each measurement, approximately 5-10 mg of the sample was accurately weighed and sealed in a 40 µL aluminium crucible. The DSC measurements were conducted under a nitrogen atmosphere with a constant purge flow rate of 50 mL/min. The temperature program involved heating the sample from 25 °C to 200 °C at a controlled rate of 10 °C/min. The glass transition temperature (T_g) of the PLA filament was subsequently determined from the DSC thermograms. This T_g value was critical in the shape-memory effect studies, as it represents the transition from a glassy to a rubbery state, which significantly influences the material's mechanical properties and its application in this study.

2.4.2 Programming of the Temporary Shape

The temporary shape programming of the eight helical models was performed using the hot programming protocol, as detailed in previous studies by Aberoumand et al. and Pandey et al. [30,31]. This protocol involved three stages:

- Heating: Each helical model was heated to a temperature above its glass transition temperature (T_g) as determined by the DSC study. In this study, two programming temperatures were selected, T_g + 5 °C (65 °C) and T_g + 10 °C (70 °C), to observe potential differences in shape-memory behaviour. At these temperatures, PLA material reached its hyperelastic state, becoming pliable enough to undergo deformation.
- Deformation and Cooling: Once the samples reached the target temperature of T_g + 5 °C and T_g + 10 °C, an external forced was applied to the helical models using calibrated weighing equipment. A 100 g weight was placed on the models for a load-holding time of 1 min, deforming the helical models from their original shape into a tablet-like temporary shape. Simultaneously, the samples were cooled to room temperature (25 ± 2 °C) while still under the applied load. This cooling process ensured the material transitioned back to its glassy state, fixing the temporary shape as the external force was removed. The shape fixity ratio (R_f), which measures the material's ability to retain the applied deformation, was then calculated using the following equation:

$$R_f = \left(\frac{L_0 - L_c}{L_0 - L_d}\right) \times 100$$

where L_0 is the initial height of the helical model, L_d is the height of the helical model after deformation, and L_c is the height of the helical model after removing the external force and cooling down. The height measurements were obtained using a digital micrometre IP65 (Mitutoyo Corporation, Kanagawa, Japan).

2.4.3 Shape Recovery Analysis

The shape recovery behaviour of the 3D-printed models was studied under conditions simulating the gastric environment. The 3D-printed models, initially in their deformed (temporary) shape, was placed into a beaker containing 500 mL of 0.01 N hydrochloric acid (HCl) at a temperature of 37 ± 2 °C. The shape changes of the 3D-printed models were observed

and recorded over a 24-hour period. The shape recovery ratio (R_r) of the 3D-printed models was calculated using the following equation:

$$R_r = \left(\frac{L_t - L_c}{L_0 - L_c}\right) \times 100$$

where L_t is the height of the 3D-printed model after recover to its original shape.

After completing the shape recovery analysis, the models that exhibited the superior shape-memory behaviour, specifically models M1 and M3, were selected for further investigations, including drug-loading performance, physicochemical properties, floatability, and release studies. This selection was based on their superior shape recovery ratios, which were key to their further applicability in gastroretentive drug delivery systems.

2.5. Drug Loading Using Soaking Method

Chlorphenamine maleate (CPM) loading was carried out by soaking the selected models (M1 and M3) in a CPM solution prepared in 95% ethanol at a concentration of 100 mg/mL. The 3D-printed models were first compressed into their temporary shape, then fully submerged in the drug solution, which was stirred magnetically at 200 rpm and room temperature for 24 h to ensure uniform drug distribution and effective loading. To avoid floating behaviour of the models during soaking, magnetic stirring was employed to maintain the complete immersion of the models in the drug solution. Additionally, beakers with dimensions appropriate to the number of models being soaked were used, ensuring uniform exposure to the solution and consistent drug loading. After soaking, the drug-loaded models were carefully removed from the solution and allowed to dry completely at room temperature (25 ± 2 °C). The drying process ensured the removal of excess solvent and preparation of the drug-loaded models for further analysis. Once dried, the drug-loaded models were stored in tight and moisture-free plastic containers at room temperature until further analysis. Once

dried, the drug-loaded models were stored in tight and moisture-free plastic containers at room temperature until further analysis.

The soaking conditions used in this study were pre-optimized based on systematic preliminary evaluations. These included assessing the effects of soaking time (6 h vs. overnight), stirring speed (non-stirring vs. stirring at 200 rpm), CPM solution concentration (50, 75, 100 mg/mL), and the solvent used for drug solution (water vs. ethanol). The conditions adopted in this study provided the best results for achieving high drug loading.

2.6. Characterisation of the Drug-Loaded models

2.6.1. Weight Variation of Drug-Loaded Models

To evaluate the reproducibility of temporary shape programming processes and ensure uniform drug distribution after drug loading via the soaking method, the weight of the drug-loaded models (M1-CPM and M3-CPM) was evaluated using the method described in Section 2.3.

2.6.2. Morphological Analysis via Scanning Electron Microscopy

The morphological characteristics of the helical parts of both drug-loaded (M1-CPM and M3-CPM) and non-drug-loaded models (M1-blank and M3-blank) were analysed using a scanning electron microscope (SEM, JCM-7000 NeoScope™ Benchtop SEM, JEOL Ltd., Tokyo, Japan). Prior to imaging, the helical parts were cut into small pieces approximately 1 cm in length and mounted on aluminium stubs using conductive double-sided adhesive carbon tape (Nisshin EM Co., Ltd., Tokyo, Japan). The samples were then gold-coated using a fully automated sputter coater (JEOL Smart Coater, JEOL Ltd., Tokyo, Japan). SEM imaging was performed in high vacuum mode with a secondary electron (SE) detector at an acceleration voltage of 10 kV. Micrographs were captured at a magnification of ×300. 2D assessments were

conducted to compare the surface and cross-sectional morphologies of the drug-loaded and non-drug-loaded 3D-printed models.

2.6.3. Quantification of Chlorpheniramine Maleate in Drug-Loaded Models

The quantification of CPM in drug-loaded models was carried out by immersing the models in 95% ethanol at room temperature (25 ± 2 °C) under continuous magnetic stirring at 100 rpm overnight, ensuring complete release of CPM. Following the extraction process, the samples were filtered using a 0.45 µm nylon syringe filter (25 mm in diameter, Labfil®, Zhejiang, China) to remove any residual particulates. The filtered samples were then diluted 40-fold with 95% ethanol to achieve the optimal concentration for analysis. The concentration of CPM in the resulting samples was determined using a UV-VIS spectrophotometer (UV-2600i, Shimadzu Corporation, Kyoto, Japan), with absorbance measured at 262.0 nm (λ_{max}). CPM content was quantified by comparing the absorbance values to a standard calibration curve, which was constructed over a concentration range of 5.0 – 60.0 µg/mL and exhibited excellent linearity with a high correlation coefficient (r^2 = 0.9986). The linear regression equation derived from the calibration curve was y = 0.0147x – 0.0386, where y represents the absorbance and x corresponds to the CPM concentration in µg/mL. The loading percentage (% w/w) of CPM in the drug-loaded models was subsequently calculated using the following equation [32]:

$$Loading\ percentage\ (\%\, w/w) = \frac{m_{CPM}}{m} \times 100$$

where m_{CPM} is the mass of CPM in drug-loaded models and m is the mass of the drug-loaded models.

2.6.4. Thermal Analysis via Differential Scanning Calorimetry

In this study, DSC was also used to evaluate the thermal properties of the drug-loaded models and CPM powder. The DSC analysis for all samples was conducted according to the methods previously described in Section 2.4.1. The glass transition temperature (T_g) was analysed, and the crystallinity percentage of each drug-loaded model was calculated using the melting enthalpy and crystallization enthalpy, as per the following equation:

$$Crystallinity\ percentage\ (\%) = \frac{\Delta H_m - \Delta H_c}{\Delta H_{m100}} \times 100$$

where ΔH_m is the melting enthalpy (J/g), ΔH_c is the crystallization enthalpy in J/g, and ΔH_{m100} is the melting enthalpy of 100% crystalline PLA, which is 93.6 J/g according to Chieng et al. [33].

2.6.5. Shape Recovery Analysis

For the shape recovery analysis of the drug-loaded models, the same method as described in Section 2.4.3 for the non-drug-loaded models was employed to assess the impact of drug incorporation on shape recovery behaviour. This approach involved subjecting the drug-loaded models to a gastric-like environment (0.01N HCl), where their recovery from a tablet-like shape (deformed state) was closely monitored and quantified.

2.6.6. Floating behaviour of Drug-Loaded Models

The floating behaviour of drug-loaded models was assessed using an *in vitro* buoyancy test. The procedure was adapted from the method described by Jiménez-Castellanos et al. [34] with modifications to align with the USP monograph for CPM tablets dissolution analysis (medium: 500 mL of 0.01 N HCl, rotation speed: 50 rpm, temperature: 37 ± 0.5 °C) [35]. Briefly, each drug-loaded model was placed in a 500 mL beaker containing 500 mL of 0.01 N HCl. The medium was maintained at 37 ± 0.5 °C using magnetic hot plate stirrer (UC152D model, Cole-Parmer® Stuart™, Vernon Hills, IL, USA) and stirred at 50 rpm. The floating lag

time, defined as the time between the introduction of the model into the medium and its rise to the surface, and the total floating time, defined as the duration for which the model remained buoyant, were both visually observed at intervals of 12 and 24 h.

2.7. In Vitro Release Study of Drug-Loaded Models

The *in vitro* release profiles of the drug-loaded models were evaluated using a USP Apparatus II (Hanson Research SR-8 Plus-85 Dissolution tester, Hanson Research Corp., Chatsworth, CA, USA) equipped with 1 L dissolution vessels and dissolution paddles. The experiments were conducted in accordance with the USP monograph for CPM tablets, using 0.01 N HCl as dissolution medium [35]. The dissolution medium was maintained at 37 ± 0.5 °C, and the paddle rotation speed was set at 50 rpm throughout the study. The release study was performed in triplicate, with 5 mL aliquots withdrawn at predetermined time intervals (1, 3, 5, 10, 15, 30 min and 1, 2, 4, 6, 8, 12 h) to assess the drug release. Each withdrawn aliquot was immediately replaced with an equal volume of fresh medium to maintain sink conditions. The withdrawn samples were filtered through a 0.45 µm nylon syringe filter, appropriately diluted, and analysed using a UV-VIS spectrophotometer (UV-2600i, Shimadzu Corporation, Kyoto, Japan) at a wavelength (λ_{max}) of 264.0 nm for quantification of the released drug. The cumulative percentage of CPM release was calculated using the standard equation derived from CPM standard curve in 0.01 N HCl: $y = 0.0216x + 0.0498$ ($r^2 = 0.9989$), where x and y correspond to CPM concentration (µg/mL) and absorbance, respectively. The cumulative percentage release was then plotted as a function of time.

2.8. Statistical Analysis

Data were analysed using SPSS Statistics software (version 17.0, SPSS Inc., Chicago, IL, USA). The results are presented as mean ± standard deviation (SD). A one-way analysis of

variance (ANOVA) was conducted to assess whether there were significant differences among the experimental results across various parameters. Bonferroni's post hoc multiple comparison test was used to identify significant differences between groups. Statistical significance was defined as $p < 0.05$

3. Results and Discussion

3.1. 3D Printing and Geometric Accuracy of 3D-Printed Helical models

This study successfully fabricated eight different helical models using the FDM technique, with each model designed based on the specific geometric parameters outlined in Table 1. As depicted in Fig. 2, the 3D-printed models generally showed high geometric accuracy, closely matching with their original CAD designs. However, some deviations were observed, particularly in models with smaller helix diameters, due to the inherent challenges in printing helical structures without the use of support 3D printing materials.

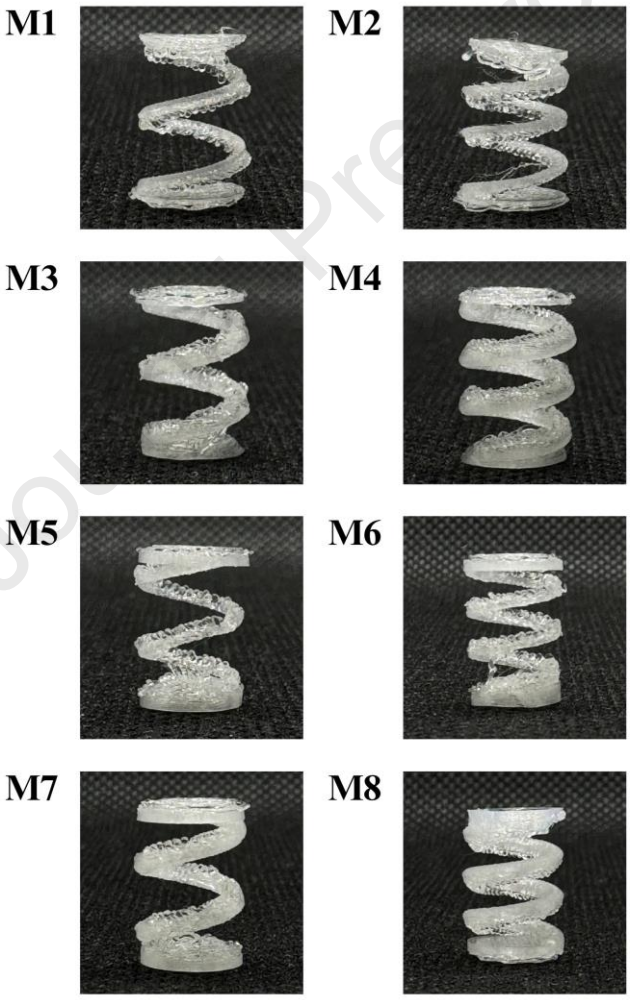

Fig. 2. Photographs of eight different 3D-printed helical models.

368 The geometric accuracy of all 3D-printed models was thoroughly evaluated with a
369 focus on the helix diameter and overall printing fidelity (Table 2). The results indicate that
370 minor deviations in printability were largely attributed to gravitational effects on the fused
371 filaments. This led to slight sagging in the helical parts of the 3D-printed models immediately
372 after filament deposition and before complete solidification, especially in the upper sections of
373 the helices. Notably, this drooping effect was less pronounced in models with larger helix
374 diameters (1.5 mm), such as M3, M4, M7, and M8, which exhibited higher printing fidelity
375 with minimal deviations. These models demonstrated reduced sagging, likely because their
376 increased diameter provided more structural stability during the printing process. In contrast,
377 models with smaller helix diameters (M1, M2, M5, and M6) showed greater variability in their
378 printed dimensions.

379 Additionally, the study found that models with a higher number of helical turns (three
380 turns) showed slightly better geometric fidelity compared to those with only two turns. These
381 findings suggest that both an increased helix diameter and a higher number of helical turns play
382 crucial roles in mitigating the drooping effect and enhancing the structural integrity of the 3D-
383 printed models. This observation aligns with prior studies that emphasize the susceptibility of
384 unsupported overhangs to gravitational effects, which cause sagging and dimensional
385 inaccuracies [36,37]. These findings highlight the necessity of incorporating support materials,
386 such as dissolvable printing materials like PVA or high-impact polystyrene (HIPS), in future
387 research to address these drooping issues. Such materials could provide temporary stabilisation
388 during the printing process and be easily removed post-production, thereby preserving the
389 intended geometry and ensuring both design fidelity and functional performance [38].

390 **Table 2.** Weight, helix diameter, and printing fidelity of the 3D-printed helical models.

Model code	Weight (mg ± SD)	Helix diameter (mm ± SD)	Printing fidelity
M1	110.7 ± 1.9 [a]	1.1 ± 0.1 [a]	1.12 ± 0.07 [a]

M2	130.1 ± 2.6 [b]	1.1 ± 0.1 [a]	1.11 ± 0.11 [a]
M3	154.0 ± 1.7 [c]	1.6 ± 0.1 [b]	1.04 ± 0.04 [b]
M4	198.5 ± 0.9 [d]	1.6 ± 0.1 [b]	1.08 ± 0.03 [b]
M5	164.4 ± 1.3 [e]	1.2 ± 0.1 [a]	1.17 ± 0.10 [a]
M6	188.4 ± 1.9 [f]	1.1 ± 0.1 [a]	1.13 ± 0.06 [a]
M7	210.4 ± 1.7 [g]	1.6 ± 0.1 [b]	1.04 ± 0.03 [b]
M8	251.0 ± 1.4 [h]	1.6 ± 0.1 [b]	1.08 ± 0.05 [b]

Note: For each test, average values with the same letter are not significantly different. Thus, average values with the different letter, e.g., 'a' or 'b' are statistically different ($p < 0.05$).

In addition to the geometric accuracy, the weight variation of the 3D-printed helical models was evaluated, with the results displayed in Table 2. The standard deviation (SD) for each model's weight was relatively narrow, indicating consistent printing accuracy and high precision in material deposition across individual samples within each model group. This narrow SD suggests that the FDM printing process maintained tight control over material extrusion, resulting in minimal weight differences within the same model design. However, despite this consistency within individual models, a significant variation in weight was observed across different models. The weight of models varied considerably, ranging from 110.7 mg for M1 to 251.0 mg for M8, reflecting the differences in geometric parameters such as helix diameter, top/base height, and number of turns. Notably, models with larger helix diameters, like M3, M4, M7, and M8, exhibited higher weight, which aligns with their more substantial structures and increased material usage. This difference in weight between models underscores the influence of geometric design on material consumption during the 3D printing process. While the FDM technique demonstrated high repeatability within each model, the variations in design parameters significantly impacted the overall material used, thus resulting in weight differences across the various models.

3.2. Thermal and Shape-Memory Performance of 3D-Printed Helical Models

411 The DSC thermogram of the PLA filament used in this study (Fig. 3) reveals the
412 material's thermal transitions, including a glass transition temperature (T_g) around 60 °C (61.42
413 °C), a cold crystallization temperature (T_c) at 99.52 °C, and a melting temperature (T_m) at
414 171.38 °C. These values are consistent with those reported in the previous literature [39],
415 confirming the thermal stability and behaviour of the PLA filament used in this study.
416 Furthermore, a strong relaxation peak was also observed in the glass transition region,
417 indicating a significant increase in polymer chain mobility as the PLA transitioned from a rigid
418 glassy state to a more flexible rubbery state. This observation suggested the onset of increased
419 molecular motion and softening of the PLA material, marking a notable change in its
420 mechanical properties.

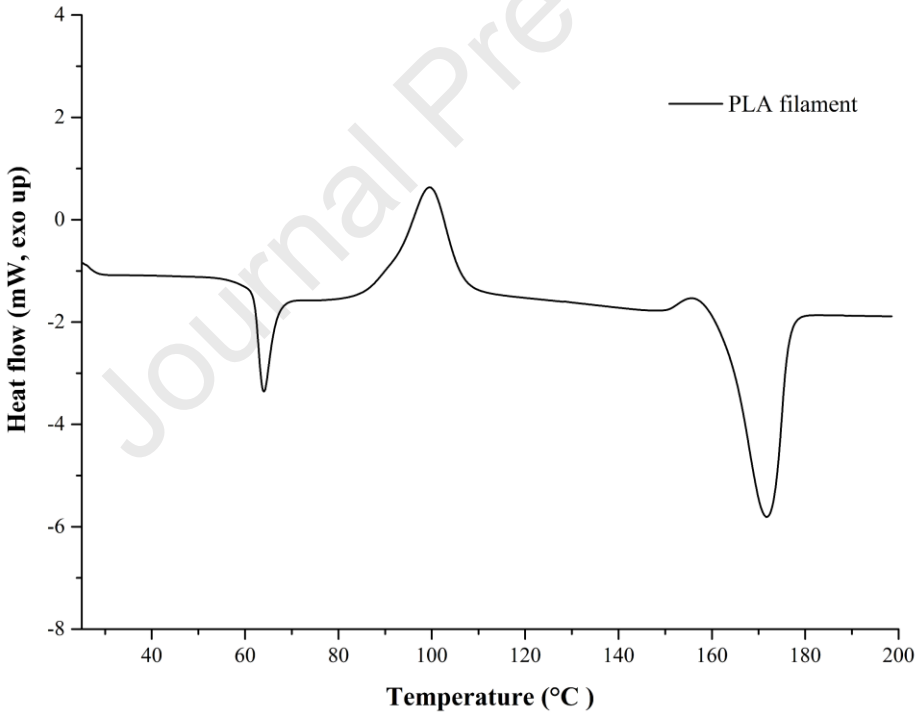

421

422 **Fig. 3.** DSC curve of PLA filament.

423 For shape-memory programming, temperatures of T_g + 5 °C (65 °C) and T_g + 10 °C
424 (70 °C) were chosen to ensure the PLA filament entered its rubbery phase, making it pliable
425 enough to be deformed into a tablet-like shape. However, experimental results showed that at

70 °C or higher, the material became too soft, causing the models to collapse into irregular shape after compression. This excessive softness also led to the helical parts sticking together excessively after compression, preventing full recovery to the original helical shape. Therefore, the 70 °C programming temperature was excluded from further analysis due to poor shape-memory performance. These findings align with the literature by Slavkovic et al. [40], which indicated that PLA's glass-to-rubber transition began at approximately 57 °C and peaked near 65 °C. This range marked a significant decrease in the elastic modulus, supporting the selection of 65 °C as the optimal programming temperature for shape-memory applications.

The shape-memory performance of the 3D-printed helical models was evaluated based on their shape fixity ratio (R_f) and shape recovery ratio (R_r). As shown in Table 3 and Fig. S1, all models demonstrated high shape fixity ratios, ranging from 96.26% to 100.78%, indicating their strong ability to retain their temporary tablet-like shape after cooling to room temperature. However, the shape recovery ratios varied significantly across the different models, illustrating the impact of geometric parameters on shape-recovery performance.

Table 3. Shape fixity at a programming temperature of 65 °C and shape recovery of eight helical models

Model code	Shape fixity ratio (R_f)	Shape recovery ratio (R_r)
M1	99.59 ± 1.64 [a]	79.52 ± 5.78 [a]
M2	100.28 ± 2.30 [a]	26.67 ± 3.01 [b]
M3	96.49 ± 2.35 [a]	51.79 ± 7.99 [c]
M4	97.22 ± 2.15 [a]	15.67 ± 4.39 [d]
M5	100.78 ± 2.18 [a]	37.81 ± 4.16 [b]
M6	98.53 ± 0.96 [a]	38.41 ± 3.64 [b]
M7	96.26 ± 0.33 [a]	35.61 ± 6.94 [b]
M8	98.37 ± 0.51 [a]	18.38 ± 4.16 [d]

Note: For each test, average values with the same letter are not significantly different. Thus, average values with the different letter, e.g., 'a' or 'b' are statistically different ($p < 0.05$).

Among the models, M1 and M3 showed the highest shape recovery ratios at 79.52% and 51.79%, respectively, indicating superior shape-memory performance. The variation in

445 shape recovery ratios across the models is likely influenced by their weight and geometric
446 parameters, such as helix diameter, number of helical turns, and top/base height. For instance,
447 M1, with a helix diameter of 1.0 mm, two helical turns, suggesting that smaller helix diameters
448 and fewer turns reduced structural resistance during recovery, enhancing the ability to return
449 to the original helical shape. Conversely, models like M4 and M8, which had larger helix
450 diameters and more helical turns, showed significantly lower shape recovery ratios (15.67%
451 and 18.38%, respectively), This suggests that increased geometric complexity adds resistance,
452 hindering shape recovery. Interestingly, models with higher top/base heights, such as M5–M8,
453 generally displayed low shape recovery ratios. This may be due to the increased weight from
454 the top part pressing down on the models, making it more difficult for the models to fully spring
455 back into helical shape. This additional pressure could reduce the models' ability to recover, as
456 more force is required to overcome the weight and structural resistance. To address this, a
457 potential solution for the further research would be to make the base heavier than the top. By
458 doing so, it would ensure that the tablet remains oriented in a vertical position, while reducing
459 the weight on the top part. This adjustment could lower the structural resistance caused by the
460 top-heavy design, thereby enhancing the shape recovery ratio and improving overall shape-
461 memory performance. By redistributing the weight more favourably, the models would require
462 less force to overcome the resistance during shape recovery.

463 These findings highlight the importance of optimising geometric parameters–such as
464 helix diameter, number of turns, and top/base height–to enhance shape recovery performance.
465 Smaller helix diameters, fewer turns, and lower top/base heights are key factors for maximizing
466 the shape recovery of PLA-based helical models. The superior shape-memory performance of
467 models M1 and M3 makes them ideal candidates for further exploration as potential drug
468 delivery systems and in other biomedical applications requiring reliable shape recovery.
469 Therefore, these two models were selected for in-depth investigation, including drug-loading

efficiency, thermal and shape-memory properties after drug loading, floatability, and release studies.

3.3. Characteristics of the Drug-Loaded Models

3.3.1. Weight Variation and Quality Control

The results indicated a significant increase in the weight of drug-loaded models compared to their non-drug-loaded counterparts in both M1 and M3 models, as shown in Table 2. Weight analysis revealed a consistent increase following drug loading in the 3D-printed helical models. For instance, the weight of model M1 increased from 110.7 ± 1.9 mg to 121.4 ± 0.7 mg, while M3's weight rose from 154.0 ± 1.7 mg to 168.0 ± 0.8 mg. This increase confirmed successful drug incorporation, validating the soaking method as an effective and reliable approach for ensuring uniform drug distribution in 3D-printed models. As critical quality attributes (CQAs) of 3D-printed drug products include weight, dimensional accuracy, and release profiles [41,42], the observed weight gain serves as a quick quality control measure. The slight weight variations between models can be attributed to differences in helix diameter and overall geometry, which influence the surface area available for drug absorption.

3.3.2. Morphological characteristics of Drug-Loaded and Non-Drug-Loaded Models

In this study, the morphological analysis of both drug-loaded and non-drug-loaded models through SEM further confirmed the efficiency of drug loading. The SEM micrographs revealed distinct differences between drug-loaded and non-drug-loaded models. As shown in Fig. 4, the non-drug-loaded models (M1-blank and M3-blank) exhibited smooth and uniform surface of the helical structures, while the drug-loaded models (M1-CPM and M3-CPM) showed a rougher texture with visible drug particles distributed across the surface and within the helix structure. This suggests that soaking method effectively facilitates drug penetration

not only on the surface but also within the inner layers of the models. The uniform distribution of the drug and the increased drug loading efficiency are crucial for sustained drug release, particularly in controlled drug delivery systems like those designed for CPM, which require frequent administration.

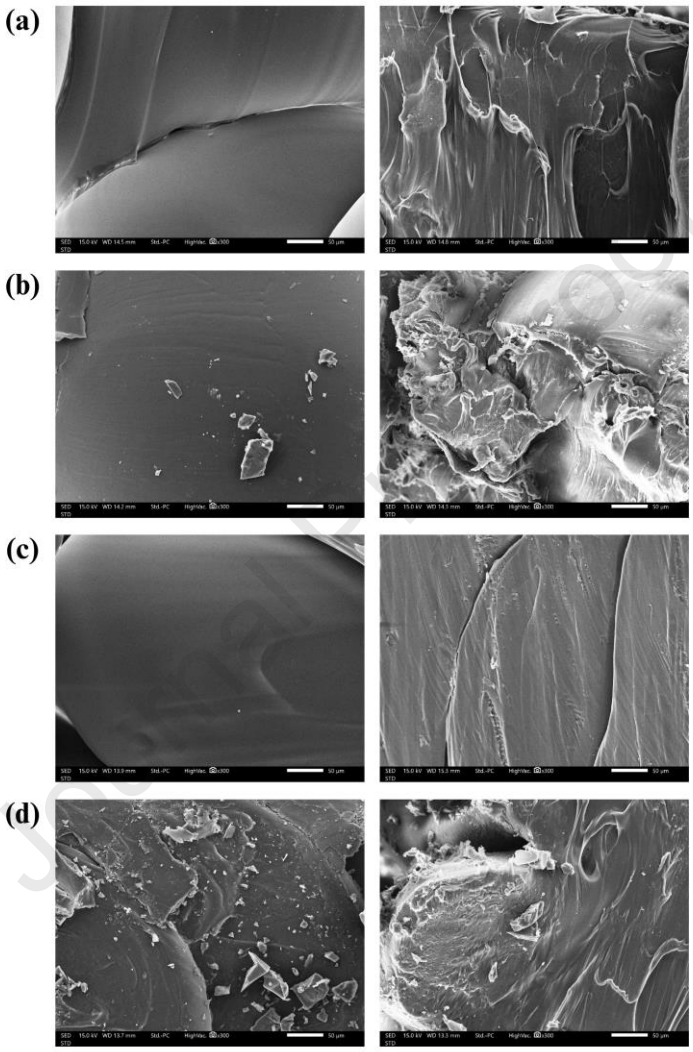

Fig. 4. Scanning electron micrographs of the surface (left) and cross-sectional (right) of (a) M1-blank, (b) M1-CPM, (c) M3-blank, and (d) M3-CPM.

3.3.3. Drug Loading Efficiency

The models demonstrated promising drug loading efficiency, with drug contents of 8.51 ± 0.46 mg in M1-CPM and 10.33 ± 0.22 mg in M3-CPM. The higher drug content in M3-CPM

compared to M1-CPM likely contributed to its larger helix diameter, as the increased surface area allows higher drug absorption. These drug amounts are sufficient to reduce the frequency of CPM administration, where the typical dose of CPM is 4 mg every 4-6 hours. The loading percentages for M1-CPM and M3-CPM were 7.01 ± 0.34% w/w and 6.15 ± 0.16% w/w, respectively, both significantly higher than those reported in previous studies [43,44], where the loading efficiency for PLA-based 3D-printed products is typically less than 2.0%. This enhanced efficiency may be attributed to the unique post-printing and post-shape-memory-programming soaking method used in this study. Unlike pre-printing drug incorporation methods, this approach allowed the drug to penetrate more effectively into the models' compressed tablet-like shape as well as remain trapped between the layers of the helix. Furthermore, the post-printing soaking process helped to avoid the high temperatures of the 3D printing process, which could otherwise degrade the drug during filament extrusion.

3.3.4. Thermal and Shape-Recovery Performance of Drug-Loaded Models

The thermal properties of PLA filament, CPM powder, and the drug loaded models (M1-CPM and M3-CPM) were assessed using DSC, with the thermograms presented in Fig, 5. The thermogram of CPM powder revealed a sharp endothermic peak at 133.11 °C, which corresponds to the CPM's melting point and indicates its crystalline structure [45,46]. Interestingly, the T_g was no longer observable in both drug-loaded models, indicating that the incorporation of CPM has disrupted the amorphous regions of the PLA matrix. This disruption is likely caused by the plasticizing effect of the CPM and possibly some residual solvent from the soaking process, which may have led to a lowering of the T_g. Furthermore, the crystallinity percentage, calculated from the area under the melting and crystallization peaks, was found to be 55.01% for M3-CPM and 19.08% for M1-CPM. These values are much higher than the crystallinity percentage of the pure unprocessed PLA filament (4.78%). The increase in

crystallinity can be ascribed to the drug incorporation process, which may have facilitated further crystallization of PLA during the soaking process. Additionally, the higher crystallinity in M3-CPM compared to M1-CPM could be due to the larger helix diameter of the M3 model, providing a greater surface area for drug absorption and subsequent crystallisation. These findings align with previous studies, where drug incorporation into PLA-based drug delivery systems and soaking process led to increased crystallinity and altered thermal properties, including the suppression or absence of glass transition endotherm [32,47,48].

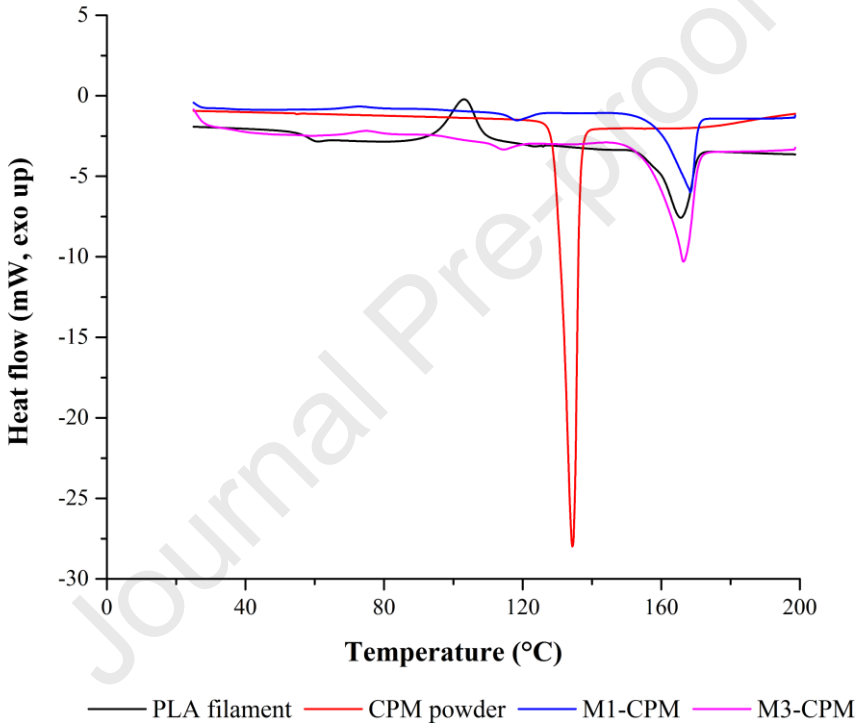

Fig. 5. DSC thermograms of PLA filament, CPM powder, and all drug-loaded models.

The shape-recovery performance of the drug-loaded models was also affected by the drug-loading process. The results showed that the shape recovery ratio (R_r) decreased in both M1-CPM and M3-CPM after drug incorporation. The R_r value for M1-CPM dropped to 21.53 ± 4.53%, while M3-CPM showed a recovery ratio of 25.59 ± 4.33% (Fig.6). This reduction in shape recovery is likely due to the increased crystallinity observed in the drug-loaded models. Higher crystallinity generally enhanceed the rigidity of the polymer matrix, making it less

flexible and more resistant to deformation. Consequently, the ability of the drug-loaded models to recover their original helical shape after deformation was restricted. Additionally, the drug incorporation may disrupt the molecular arrangement of PLA, further hindering the shape-recovery effect. These findings are consistent with previous research on SMP-based controlled drug delivery system, which found that high drug loading caused the polymer networks to lose their elasticity and flexibility, preventing them from being programmed into a temporary shape or recovered to their original shape [49]. This suggests that it is essential to determine the optimal drug loading level to preserve shape-memory performances, which should be considered in future studies.

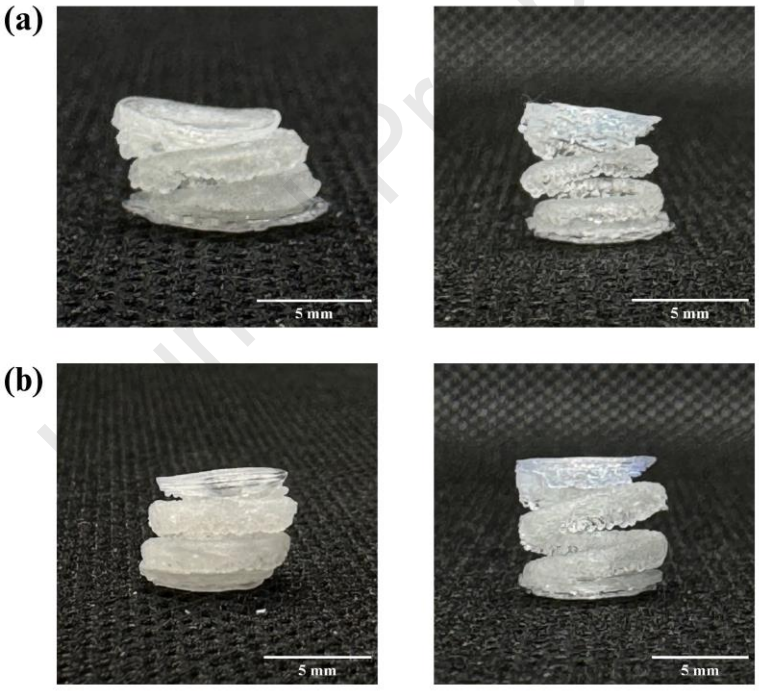

Fig. 6. Photographs of drug-loaded models M1-CPM (a) and M3-CPM (b) showing their appearance after shape programming and drug loading (left) and after shape recovery (right).

3.3.5. Floating Ability of Drug-Loaded Models

This study examined the floatability of the two drug-loaded models, M1-CPM and M3-CPM, under simulated gastric conditions to evaluate their suitability for gastric retention. The

562 *in vitro* buoyancy test demonstrated that both models exhibited immediate floating in a 0.01 N
563 HCl solution without any floating lag time and maintained buoyancy for 12 h (Fig. S2). The
564 densities of M1 and M3 models were calculated to be 1.43 g/cm^3 and 1.31 g/cm^3, respectively,
565 both of which slightly higher than that of gastric fluid (approximately 1.004 – 1.010 g/cm^3)
566 [50]. This allows the models to be eliminated from the body by peristalsis of the gastrointestinal
567 (GI) tract. Despite their higher densities, the models initially floated because of their special
568 structural design. One possible explanation for the buoyancy of M1-CPM and M3-CPM is the
569 presence of air trapped within their helical structure when they are compressed into a temporary
570 tablet-like shape during shape-memory programming. The hollow design of the helix naturally
571 creates internal cavities that trap air, even when immersed in the 0.01 N HCl solution. This
572 trapped air prevents water from completely filling the internal cavities, significantly reducing
573 the overall effective density of the models and allowing them to float [51,52]. Furthermore, the
574 helical structure, specifically designed to have the same diameters and height at the top and
575 base, provides stability for floating. Additionally, the relatively hydrophobic nature of the PLA
576 material further minimised water absorption, enabling the models to stay buoyant for longer
577 periods. However, this study found that the floating behaviour of both models was not sustained
578 beyond 24 h, as some constructs began to sink. The loss of buoyancy in the models at 24 h may
579 be attributed to the gradual penetration of water into the internal helical cavities or the diffusion
580 of air. Overall, this work highlights the importance of geometric design, material choice, and
581 air-trapping capabilities in the development of effective floating drug delivery systems.
582
583 *3.4. In Vitro CPM release profiles*
584 The *in vitro* release profiles of CPM from the drug-loaded models (M1-CPM and M3-
585 CPM) were studied over a 12-hour period, based on how they floated in the simulated gastric
586 environment. As shown in Fig. 7, both models displayed a biphasic release pattern,

587 characterised by an initial rapid burst release phase followed by a gradually sustained release
588 phase. The initial burst in both models could be attributed to the rapid dissolution of CPM that
589 are on the surface of the helical structures. This effect is frequently observed in drug delivery
590 systems where surface-bound drug particles dissolve quickly upon contact with the dissolution
591 media [53,54]. The release rate during this phase was significantly faster for M3-CPM in
592 comparison to M1-CPM, most likely because of the larger helix diameter and greater surface
593 area of M3 model. This increased surface area in M3-CPM facilitated higher drug interaction
594 with the media, thus leading to quicker dissolution of CPM.

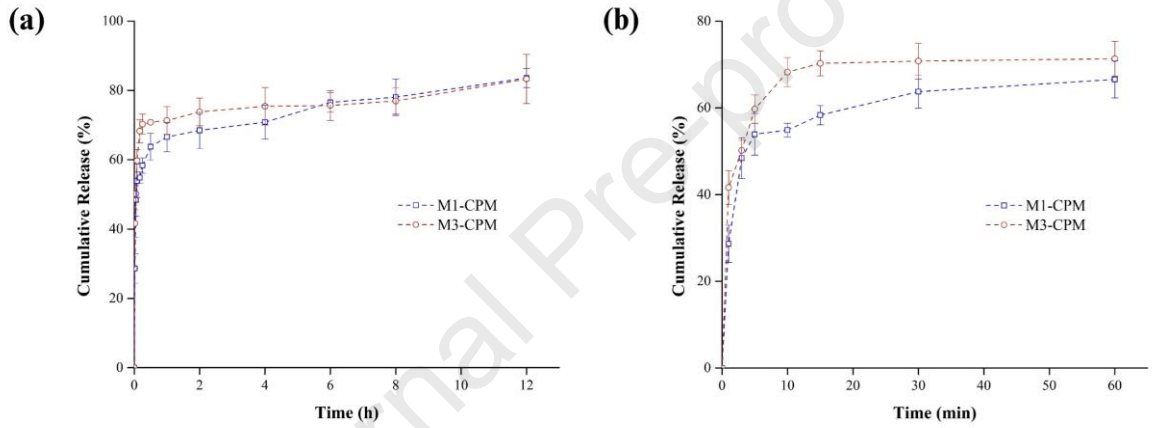

595

596 **Fig. 7.** *In vitro* CPM release profiles of M1-CPM and M3-CPM over 12 h (a) and during the first hour (b).

597 Following the initial rapid release in the first few hours, the drug release from both
598 models shifted to a sustained phase. During this phase, the release rates between the two models
599 became comparable, with both reaching approximately 83% cumulative drug release by the
600 end of the 12-hour study. This prolonged release phase may be attributed to the limited
601 availability of surface-bound CPM, resulting in the drug being gradually released through
602 diffusion from the inner layers of the helical structures. Furthermore, the slower release pattern
603 observed in M3-CPM during this phase can also attributed to its increased crystallinity, as
604 demonstrated by prior DSC findings that indicated a larger percentage of crystallinity in M3-
605 CPM compared to M1-CPM. Additionally, the hydrophobic nature of PLA may also slow the

penetration of water into the inner layers of the constructs, thereby prolonging the release of CPM. The observed biphasic release pattern in this study has significant implications for design and development of GRDDS. The initial burst release phase can be useful for achieving a rapid therapeutic effect, whilst the subsequent sustained release phase can assist in maintaining drug levels within the therapeutic range over an extended period. Unlike conventional floating drug delivery systems, which often depend on gastric pH or gastric fluid–factors that vary widely between patients–the PLA-based 4D-printed tablets in this study are designed to respond to body temperature. The nearly uniform temperature of approximately 37 °C across patients ensures predictable activation of the shape-memory properties, minimising variability in shape-changing behaviour and drug release profiles. This could make PLA-based 4D drug delivery systems a more reliable alternative to conventional floating tablets, particularly in clinical practices. While direct comparisons with conventional drug delivery systems were not within the scope of this study, these factors should be considered in future research to further evaluate the advantages of this 4D-printed GRDDS.

4. Conclusion

In summary, this study successfully demonstrates the concept of 4D printing in drug delivery through the fabrication of eight different helical models capable of changing shape upon contact with specific stimuli. These models were created with high geometric accuracy using FDM technology. The thermal and shape-memory performance studies of these models revealed the significant impact of geometric parameters, such as helix diameter and number of turns, on shape recovery performance. Larger helix diameters and more helical turns exhibited higher geometric fidelity but lower shape recovery due to the increase in structural complexity and compression from their own weight. After drug loading, both M1-CPM and M3-CPM models exhibited effective drug loading efficiencies and sustained release profiles with a biphasic release pattern. This included an initial rapid drug release within the first few hours, followed by a prolonged release phase lasting up to 12 h, during which approximately 83% of the drug was released. These findings highlight the potential of these models for use in GRDDS, offering prolonged gastric retention through buoyancy and sustained drug release. A key strength of the PLA-based 4D-printed drug delivery system is its activation by body temperature–a stable and consistent physiological parameter–rather than gastric fluid properties, which can vary significantly among patients. This predictability enhances the drug delivery system's reliability and makes it a promising candidate for floating drug delivery applications. However, future studies should consider incorporating direct comparisons with conventional drug delivery systems to better evaluate potential benefits of these 4D-printed GRDDS. Additionally, this study also showed some limitations, such as the decrease in shape recovery performance after drug loading and a floating ability limited to 12 h. To address these challenges, further research should explore alternative materials or polymer blends to enhance both shape recovery and release behaviour. Moreover, modifications to the geometric structures should be considered to enable the models to float for up to 24 h, allowing for once-

645 daily dosing, which would improve patient compliance and therapeutic outcomes. With further
646 optimisation in material selection and design, these 4D-printed drug delivery systems hold
647 promise as advanced GRDDS platforms, representing a significant step forward in the
648 application of 4D printing in pharmaceutical field.

Funding

This research project was supported by Faculty of Pharmacy, Chiang Mai University and was part of the Big Bang International Projects between Chiang Mai University and University of East Anglia.

CRediT authorship contribution statement

P. Panraksa: Conceptualization, Formal Analysis, Investigation, Methodology, Project administration, Writing – original draft, Writing – review & editing. **S. Hamdallah:** Investigation, Supervision, Writing – review & editing. **O. Yilmaz:** Investigation, Methodology, Writing – original draft. **P. Saokham:** Investigation, Methodology, Writing – review & editing. **P. Rachtanapun:** Investigation, Methodology, Writing – review & editing. **S. Qi:** Investigation, Supervision, Writing – review & editing. **P. Jantrawut:** Conceptualization, Investigation, Methodology, Supervision, Writing – original draft, Writing – review & editing. All the authors contributed to the realisation of the manuscript and have given approval to the final version of the manuscript.

Declaration of Competing Interest

The authors declare that they have no known competing financial interests or personal relationships that could have appeared to influence the work reported in this paper.

Acknowledgements

The authors would like to thank and gratefully acknowledge Chattarin Sapso, Natthanicha Sukprapaporn, Pran Thamvivornkul, and Saktiyaphong Paowan for their assistance in conducting the experiments for this research project. The present study was

673 partially supported by Chiang Mai University and Thailand Research Fund (TRF) Research
674 Team Promotion Grant, RTA, Senior Research Scholar (N42A671052).

675 **References**

676 [1] N. Debotton, A. Dahan, Applications of polymers as pharmaceutical excipients in solid oral
677 dosage forms, Med. Res. Rev. 37 (2017) 52–97. https://doi.org/10.1002/med.21403.

678 [2] Y.T. Mekasha, Pharmaceutical solid oral dosage form analysis: Literature review, Open Access
679 J. Biog. Sci. Res. 4 (2020) 1–9. https://doi.org/10.46718/jbgsr.2020.04.000087.

680 [3] T. Kimura, K. Higaki, Gastrointestinal transit and drug absorption, Biol. Pharm. Bull. 25 (2002)
681 149–164. https://doi.org/10.1248/bpb.25.149.

682 [4] B. Homayun, X. Lin, H.J. Choi, Challenges and recent progress in oral drug delivery systems
683 for biopharmaceuticals, Pharmaceutics. 11 (2019) 129.
684 https://doi.org/10.3390/pharmaceutics11030129.

685 [5] L.M. Ensign, R. Cone, J. Hanes, Oral drug delivery with polymeric nanoparticles: The
686 gastrointestinal mucus barriers, Adv. Drug Deliv. Rev. 64 (2012) 557–570.
687 https://doi.org/10.1016/j.addr.2011.12.009.

688 [6] J.B. Dressman, R.R. Berardi, L.C. Dermentzoglou, T.L. Russell, S.P. Schmaltz, J.L. Barnett,
689 K.M. Jarvenpaa, Upper gastrointestinal (GI) pH in young, healthy men and women, Pharm. Res.
690 7 (1990) 756–761. https://doi.org/10.1023/A:1015827908309.

691 [7] N. Rouge, P. Buri, E. Doelker, Drug absorption sites in the gastrointestinal tract and dosage
692 forms for site-specific delivery, Int. J. Pharm. 136 (1996) 117–139.
693 https://doi.org/10.1016/0378-5173(96)85200-8.

694 [8] Nayak A. K., Malakar J., Sen K. K., Gastroretentive drug delivery technologies: Current
695 approaches and future potential, J. Pharm. Educ. Res. 1 (2010) 1.

696 [9] G.M. Clarke, J.M. Newton, M.D. Short, Gastrointestinal transit of pellets of differing size and
697 density, Int. J. Pharm. 100 (1993) 81–92. https://doi.org/10.1016/0378-5173(93)90078-T.

698 [10] M. Neumann, C. Heimhardt, K. Seidlitz, M. Koziolek, F. Schneider, C. Schiller, U. Hanke, M.
699 Anschütz, C. Knopke, F. Donath, R. Thoma, C. Brätter, B. Schug, H. Franke, W. Weitschies,
700 Development of a furosemide-containing expandable system for gastric retention, J. Control.
701 Release. 338 (2021) 105–118. https://doi.org/10.1016/j.jconrel.2021.08.026.

702 [11] L.A. Corá, F.G. Romeiro, M.F. Américo, R.B. Oliveira, O. Baffa, M. Stelzer, J.R. De Arruda

Miranda, Gastrointestinal transit and disintegration of enteric coated magnetic tablets assessed by ac biosusceptometry, Eur. J. Pharm. Sci. 27 (2006) 1–8. https://doi.org/10.1016/j.ejps.2005.08.009.

[12] M.R. Bhalekar, R. V. Bargaje, P.G. Upadhaya, A.R. Madgulkar, S.J. Kshirsagar, Formulation of mucoadhesive gastric retentive drug delivery using thiolated xyloglucan, Carbohydr. Polym. 136 (2016) 537–542. https://doi.org/10.1016/j.carbpol.2015.09.064.

[13] V.A. Eberle, J. Schoelkopf, P.A.C. Gane, R. Alles, J. Huwyler, M. Puchkov, Floating gastroretentive drug delivery systems:Comparison of experimental and simulated dissolution profiles and floatation behavior, Eur. J. Pharm. Sci. 58 (2014) 34–43. https://doi.org/10.1016/j.ejps.2014.03.001.

[14] A. Raza, N. Shen, J. Li, Y. Chen, J.Y. Wang, Formulation of zein based compression coated floating tablets for enhanced gastric retention and tunable drug release, Eur. J. Pharm. Sci. 132 (2019) 163–173. https://doi.org/10.1016/j.ejps.2019.01.025.

[15] A. Streubel, J. Siepmann, R. Bodmeier, Floating matrix tablets based on low density foam powder: Effects of formulation and processing parameters on drug release, Eur. J. Pharm. Sci. 18 (2003) 37–45. https://doi.org/10.1016/S0928-0987(02)00223-3.

[16] S. Treesinchai, S. Puttipipatkhachorn, T. Pitaksuteepong, S. Sungthongjeen, Development of curcumin floating tablets based on low density foam powder, Asian J. Pharm. Sci. 11 (2016) 130–131. https://doi.org/10.1016/j.ajps.2015.11.092.

[17] G. Chen, Y. Xu, P.C.L. Kwok, L. Kang, Pharmaceutical applications of 3D printing, Addit. Manuf. 34 (2020) 101209. https://doi.org/10.1016/j.addma.2020.101209.

[18] J. Mancilla-De-la-Cruz, M. Rodriguez-Salvador, J. An, C.K. Chua, Three-dimensional printing technologies for drug delivery applications: Processes, materials, and effects, Int. J. Bioprinting. 8 (2022) 622. https://doi.org/10.18063/ijb.v8i4.622.

[19] S.J. Trenfield, A. Awad, A. Goyanes, S. Gaisford, A.W. Basit, 3D printing pharmaceuticals: drug development to frontline care, Trends Pharmacol. Sci. 39 (2018) 440–451. https://doi.org/10.1016/j.tips.2018.02.006.

[20] A. Mahmood, T. Akram, C. Shenggui, H. Chen, Revolutionizing manufacturing: A review of

4D printing materials, stimuli, and cutting-edge applications, Compos. Part B Eng. 266 (2023) 110952. https://doi.org/10.1016/j.compositesb.2023.110952.

[21] S.K. Leist, J. Zhou, Current status of 4D printing technology and the potential of light-reactive smart materials as 4D printable materials, Virtual Phys. Prototyp. 11 (2016) 249–262. https://doi.org/10.1080/17452759.2016.1198630.

[22] D. Kim, K.H. Kim, Y.S. Yang, K.S. Jang, S. Jeon, J.H. Jeong, S.A. Park, 4D printing and simulation of body temperature-responsive shape-memory polymers for advanced biomedical applications, Int. J. Bioprinting. 10 (2024) 3035. https://doi.org/10.36922/ijb.3035.

[23] N. Inverardi, G. Scalet, A. Melocchi, M. Uboldi, A. Maroni, L. Zema, A. Gazzaniga, F. Auricchio, F. Briatico-Vangosa, F. Baldi, S. Pandini, Experimental and computational analysis of a pharmaceutical-grade shape memory polymer applied to the development of gastroretentive drug delivery systems, J. Mech. Behav. Biomed. Mater. 124 (2021) 104814. https://doi.org/10.1016/j.jmbbm.2021.104814.

[24] Q. Ge, A.H. Sakhaei, H. Lee, C.K. Dunn, N.X. Fang, M.L. Dunn, Multimaterial 4D printing with tailorable shape memory polymers, Sci. Rep. 6 (2016) 31110. https://doi.org/10.1038/srep31110.

[25] A.U. Vakil, M. Ramezani, M.B.B. Monroe, Magnetically actuated shape memory polymers for on-demand drug delivery, Materials (Basel). 15 (2022) 7279. https://doi.org/10.3390/ma15207279.

[26] M.D. Hager, S. Bode, C. Weber, U.S. Schubert, Shape memory polymers: Past, present and future developments, Prog. Polym. Sci. 49 (2015) 3–33. https://doi.org/10.1016/j.progpolymsci.2015.04.002.

[27] M. Uboldi, C. Perrotta, C. Moscheni, S. Zecchini, A. Napoli, C. Castiglioni, A. Gazzaniga, A. Melocchi, L. Zema, Insights into the safety and versatility of 4D printed intravesical drug delivery systems, Pharmaceutics. 15 (2023) 757. https://doi.org/10.3390/pharmaceutics15030757.

[28] A. Melocchi, M. Uboldi, N. Inverardi, F. Briatico-Vangosa, F. Baldi, S. Pandini, G. Scalet, F. Auricchio, M. Cerea, A. Foppoli, A. Maroni, L. Zema, A. Gazzaniga, Expandable drug delivery

system for gastric retention based on shape memory polymers: Development via 4D printing and extrusion, Int. J. Pharm. 571 (2019) 118700. https://doi.org/10.1016/j.ijpharm.2019.118700.

[29] C. Cappellini, Y. Borgianni, L. Maccioni, C. Nezzi, The effect of process parameters on geometric deviations in 3D printing with fused deposition modelling, Int. J. Adv. Manuf. Technol. 122 (2022) 1763–1803. https://doi.org/10.1007/s00170-022-09924-4.

[30] M. Aberoumand, K. Soltanmohammadi, D. Rahmatabadi, E. Soleyman, I. Ghasemi, M. Baniassadi, K. Abrinia, M. Bodaghi, M. Baghani, 4D printing of polyvinyl chloride (PVC): A detailed analysis of microstructure, programming, and shape memory performance, Macromol. Mater. Eng. 308 (2023) 2200677. https://doi.org/10.1002/mame.202200677.

[31] H. Pandey, S.S. Mohol, R. Kandi, 4D printing of tracheal scaffold using shape-memory polymer composite, Mater. Lett. 329 (2022) 133238. https://doi.org/10.1016/j.matlet.2022.133238.

[32] J. Kukkonen, T. Ervasti, R. Laitinen, Production and characterization of glibenclamide incorporated PLA filaments for 3D printing by fused deposition modeling, J. Drug Deliv. Sci. Technol. 77 (2022) 103843. https://doi.org/10.1016/j.jddst.2022.103843.

[33] B.W. Chieng, N.A. Ibrahim, W.M.Z.W. Yunus, M.Z. Hussein, Poly(lactic acid)/poly(ethylene glycol) polymer nanocomposites: Effects of graphene nanoplatelets, Polymers (Basel). 6 (2014) 93–104. https://doi.org/10.3390/polym6010093.

[34] M.R. Jiménez-Castellanos, H. Zia, C.T. Rhodes, Design and testing in vitro of a bioadhesive and floating drug delivery system for oral application, Int. J. Pharm. 105 (1994) 65–70. https://doi.org/10.1016/0378-5173(94)90236-4.

[35] Monograph: USP. Chlorpheniramine maleate tablets, in: United States Pharmacop. (USP43 NF38), The United States Pharmacopeial Convention, Rockville, MD, USA, 2019: p. 971. https://doi.org/10.31003/USPNF_M16490_01_01.

[36] Y. Zhou, X. Xia, X. Liu, B. Huang, L. Xiao, Q. Qian, Q. Chen, Preparation and rheological and mechanical properties of poly(butylene succinate)/talc composites for material extrusion additive manufacturing, Macromol. Mater. Eng. 304 (2019) 1900021. https://doi.org/10.1002/mame.201900021.

[37] D. Jiang, F. Ning, Anisotropic deformation of 316L stainless steel overhang structures built by

material extrusion based additive manufacturing, Addit. Manuf. 50 (2022) 102545. https://doi.org/10.1016/j.addma.2021.102545.

[38] S.J. Park, J.E. Lee, J.H. Park, N.K. Lee, M.Y. Lyu, K. Park, M.S. Koo, S.H. Cho, Y. Son, S.H. Park, Enhanced solubility of the support in an FDM-based 3D printed structure using hydrogen peroxide under ultrasonication, Adv. Mater. Sci. Eng. 1 (2018) 3018761. https://doi.org/10.1155/2018/3018761.

[39] B.D.M. Matos, V. Rocha, E.J. da Silva, F.H. Moro, A.C. Bottene, C.A. Ribeiro, D. dos Santos Dias, S.G. Antonio, A.C. do Amaral, S.A. Cruz, H.G. de Oliveira Barud, H. da Silva Barud, Evaluation of commercially available polylactic acid (PLA) filaments for 3D printing applications, J. Therm. Anal. Calorim. 137 (2019) 555–562. https://doi.org/10.1007/s10973-018-7967-3.

[40] V. Slavković, B. Hanželič, V. Plesec, S. Milenković, G. Harih, Thermo-mechanical behavior and strain rate sensitivity of 3D-printed polylactic acid (PLA) below glass transition temperature (Tg), Polymers (Basel). 16 (2024) 1526. https://doi.org/10.3390/polym16111526.

[41] J. Zhang, R. Thakkar, Y. Zhang, M. Maniruzzaman, Structure-function correlation and personalized 3D printed tablets using a quality by design (QbD) approach, Int. J. Pharm. 590 (2020) 119945. https://doi.org/10.1016/j.ijpharm.2020.119945.

[42] S. Henry, L. De Wever, V. Vanhoorne, T. De Beer, C. Vervaet, Influence of print settings on the critical quality attributes of extrusion-based 3d-printed caplets: A quality-by-design approach, Pharmaceutics. 13 (2021) 2068. https://doi.org/10.3390/pharmaceutics13122068.

[43] X. Farto-vaamonde, G. Auriemma, R. Patrizia, A. Concheiro, C. Alvarez-lorenzo, Post-manufacture loading of filaments and 3D printed PLA scaffolds with prednisolone and dexamethasone for tissue regeneration applications, Eur. J. Pharm. Biopharm. 141 (2019) 100–110. https://doi.org/10.1016/j.ejpb.2019.05.018.

[44] J.R. Cerda, T. Arifi, S. Ayyoubi, P. Knief, M.P. Ballesteros, W. Keeble, E. Barbu, A.M. Healy, A. Lalatsa, D.R. Serrano, Personalised 3D printed medicines : Optimising material properties for successful passive diffusion loading of filaments for fused deposition modelling of solid dosage forms, Pharmaceutics. 12 (2020) 345. https://doi.org/10.3390/pharmaceutics12040345.

[45] C.G. Eckhart, T. McCorkle, Chlorpheniramine Maleate, in: Anal. Profiles Drug Subst. Excipients, 1978: pp. 43–80. https://doi.org/10.1016/S0099-5428(08)60089-1.

[46] G.G.G. de Oliveira, A. Feitosa, K. Loureiro, A.R. Fernandes, E.B. Souto, P. Severino, Compatibility study of paracetamol, chlorpheniramine maleate and phenylephrine hydrochloride in physical mixtures, Saudi Pharm. J. 25 (2017) 99–103. https://doi.org/10.1016/j.jsps.2016.05.001.

[47] N. Naga, Y. Yoshida, K. Noguchi, S. Murase, Crystallization of amorphous poly(lactic acid) induced by vapor of acetone to form high crystallinity and transparency specimen, Open J. Polym. Chem. 3 (2013) 29–33. https://doi.org/10.4236/ojpchem.2013.32006.

[48] S. Sato, D. Gondo, T. Wada, S. Kanehashi, K. Nagai, Effects of various liquid organic solvents on solvent-induced crystallization of amorphous poly(lactic acid) film, J. Appl. Polym. Sci. 129 (2013) 1607–1617. https://doi.org/10.1002/app.38833.

[49] K. Nagahama, Y. Ueda, T. Ouchi, Y. Ohya, Biodegradable shape-memory polymers exhibiting sharp thermal transitions and controlled drug release, Biomacromolecules. 10 (2009) 1789–1794. https://doi.org/10.1021/bm9002078.

[50] M.S. Chauhan, A. Kumar, K. Pathak, Osmotically regulated floating asymmetric membrane capsule for controlled site-specific delivery of ranitidine hydrochloride: Optimization by central composite design, AAPS PharmSciTech. 13 (2012) 1492–1501. https://doi.org/10.1208/s12249-012-9870-8.

[51] X. Chai, H. Chai, X. Wang, J. Yang, J. Li, Y. Zhao, W. Cai, T. Tao, X. Xiang, Fused deposition modeling (FDM) 3D printed tablets for intragastric floating delivery of domperidone, Sci. Rep. 7 (2017) 2829. https://doi.org/10.1038/s41598-017-03097-x.

[52] S. Shin, T.H. Kim, S.W. Jeong, S.E. Chung, D.Y. Lee, D. Kim, B.S. Shin, Development of a gastroretentive delivery system for acyclovir by 3D printing technology and its in vivo pharmacokinetic evaluation in Beagle dogs, PLoS One. 14 (2019) e0216875. https://doi.org/10.1371/journal.pone.0216875.

[53] H.O. Ammar, M. Ghorab, R. Kamel, A.H. Salama, Design and optimization of gastro-retentive microballoons for enhanced bioavailability of cinnarizine, Drug Deliv. Transl. Res. 6 (2016)

210–224. https://doi.org/10.1007/s13346-016-0280-4.

[54] A. Ismail, M. Teiama, B. Magdy, W. Sakran, Development of a novel bilosomal system for improved oral bioavailability of sertraline hydrochloride: Formulation design, in vitro characterization, and ex vivo and in vivo studies, AAPS PharmSciTech. 23 (2022) 188. https://doi.org/10.1208/s12249-022-02339-0.

Supplementary Materials: 4D Printing of Shape-Memory Polymer-Based Floating Tablets via Fused Deposition Modelling: Transformable Helical Structure to Tablet-Like Form

Pattaraporn Panraksa [a], Sherif Hamdallah [b], Ozkan Yilmaz [b], Phennapha Saokham [a], Pornchai Rachtanapun [c,d,e], Sheng Qi [b], and Pensak Jantrawut [a,d,e,*]

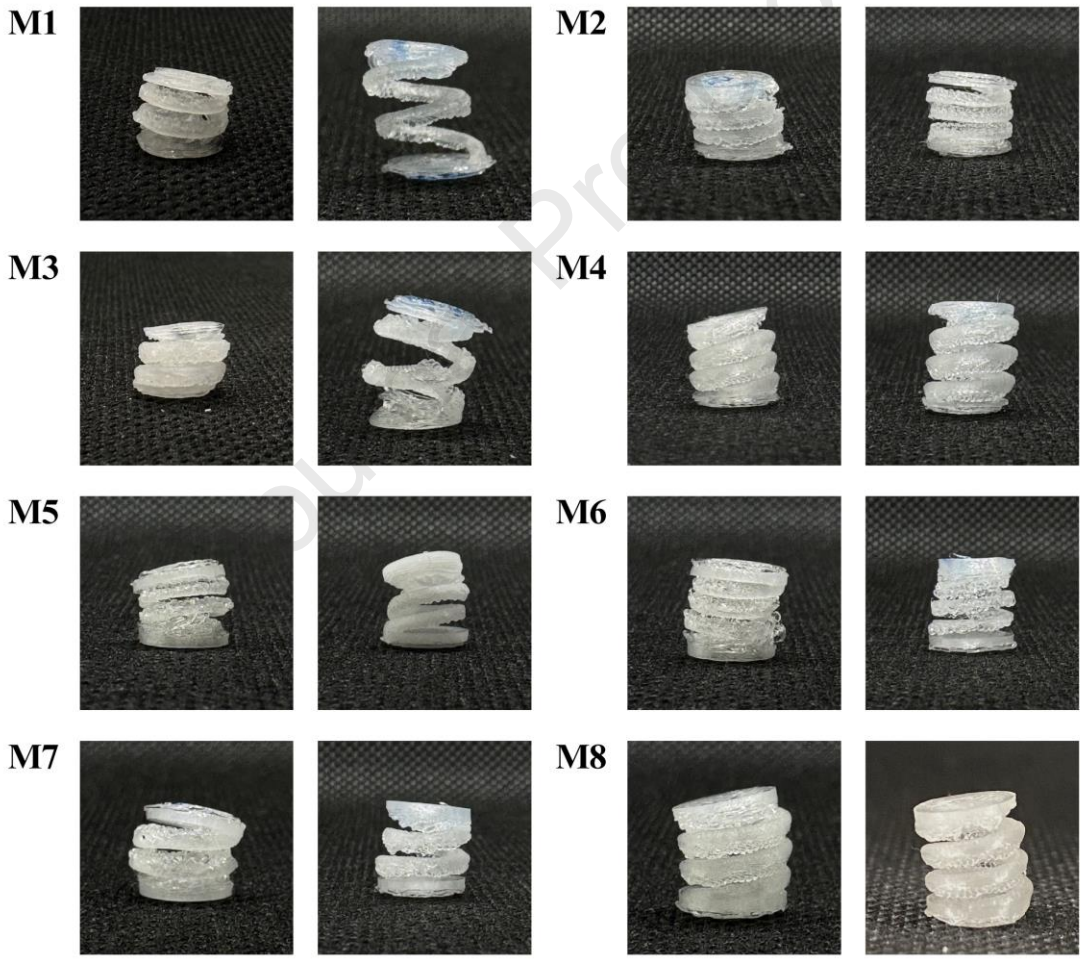

Fig. S1. Photographs of all models showing their appearance after shape programming (left) and after shape recovery (right).

Fig. S2. Model floating in 0.01 N HCl after 12 h.

Declaration of interests

☒ The authors declare that they have no known competing financial interests or personal relationships that could have appeared to influence the work reported in this paper.